JOURNAL OF CHEMICAL INFORMATION AND MODELING

Article

pubs.acs.org/jcim

Structural and Energetic Analyses of SNPs in Drug Targets and Implications for Drug Therapy

Hui-Yong Sun,[†,‡,§,∥] Feng-Qin Ji,[†,§,⊥] Liang-Yu Fu,[†] Zhong-Yi Wang,[†] and Hong-Yu Zhang*[,†]

[†]National Key Laboratory of Crop Genetic Improvement, Center for Bioinformatics, College of Life Science and Technology, Huazhong Agricultural University, Wuhan 430070, P.R. China

[‡]School of Life Sciences, Shandong University of Technology, Zibo 255049, P.R. China

Supporting Information

ABSTRACT: Mutations in drug targets can alter the therapeutic effects of drugs. Therefore, evaluating the effects of single-nucleotide polymorphisms (SNPs) on drug-target binding is of significant interest. This study focuses on the analysis of the structural and energy properties of SNPs in successful drug targets by using the data derived from HapMap and the Therapeutic Target Database. The results show the following: (i) Drug targets undergo strong purifying selection, and the majority (92.4%) of the SNPs are located far from the drug-binding sites (>12 Å). (ii) For SNPs near the drug-binding pocket (≤12 Å), nearly half of the drugs are weakly affected by the SNPs, and only a few drugs are significantly affected by the target mutations. These results have direct implications for population-based drug therapy and for chemical treatment of genetic diseases as well.

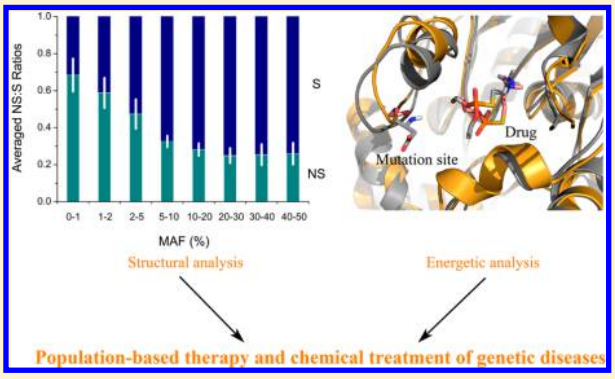

INTRODUCTION

Chemical drugs generally exhibit therapeutic effects by binding with biological macromolecules (drug targets), particularly proteins. However, different individuals have different genotypes because of spontaneous gene mutations. Nonsynonymous mutations that occur in drug targets can affect drug binding, thereby influencing drug effects. For instance, break point cluster-Abelson tyrosine kinase (BCR-ABL) is a target for chronic leukemia therapy. The T315I mutation in the ABL domain of the target leads to the loss of an important hydrogen bond between the target and the drug STI-571, which induces drug resistance.[1] The epidermal growth factor receptor is a target for nonsmall cell lung carcinoma (NSCLC) therapy. The T790 M mutation in the target causes drug resistance to gefitinib by enhancing the binding affinity of the substrate ATP,[2] thereby weakening the competitiveness of the inhibitor. Crizotinib is a drug for the treatment of fusion-type NSCLC and targets echinoderm microtubule-associated protein-like 4-anaplastic lymphoma kinase (ALK). The L1196M, C1156Y, and G1202R mutations in the ALK domain of the target cause drug resistance by preventing the entrance of crizotinib into the active pocket,[3] decreasing the nonbonded interactions between crizotinib and the target[4] and hindering the binding of the drug to the binding channel.[5] The mutations can also occur in transporters that mediate the uptake and efflux of xenobiotics (toxins, carcinogens, and drugs), thereby causing multidrug resistance. Previous studies have shown that a large number of drug resistance cases are related to transporter mutations.[6,7]

The Human Genome Project has shown that more than 1.4 million single-nucleotide polymorphisms (SNPs) exist in the human genome.[8] In addition, approximately 60,000 SNPs are located in the coding regions.[9] Apparently, target mutations may affect drug effects. Therefore, evaluating the effects of SNPs on drug-target binding has gained significant interest and has inspired our group to conduct a comprehensive analysis on the structural features of SNPs in drug targets and their effects on drug binding affinities. The results will have important implications for drug therapy.

MATERIALS AND METHODS

Data Preparation. First, information on successful drug targets were extracted from the Therapeutic Target Database (TTD).[10] Second, the *Blastp* program in NCBI[11] was employed to obtain the crystal structures of the drug targets with 100% similarity to the query sequence. The information related to mutations (SNP sites with RS ID) and their frequencies in different populations were also collected from Uniprot[12] and HapMap.[13] Third, the SNP sites were mapped into the successful drug targets, and the minimum distance between the SNP site and the active pocket (characterized by the distance between heavy atoms in the mutated residue and the docked drug) was measured. The measurement strategy is detailed below.

Received: August 1, 2013
Published: December 4, 2013

Table 1. Basic Information of 12 Drug Targets with SNPs Close to Corresponding Drugs

target name	RS ID	SNP site	PDB ID and redocking RMSD[a] (Å)	drug name	distance between mutated site and drug (Å)	binding free energy[b] (kcal/mol)		
						ΔG_{WT}	ΔG_{MT}	$\Delta\Delta G$
cytochrome P450 3A4 (CYP3A4)	rs12721629	L373F	1TQN[c]	clotrimazole (inhibitor)	6.7	−11.89	−11.48	0.41
peroxisome proliferator activated receptor alpha (PPARα)	rs1042311	A268 V	1I7G (0.82)	AD-4833 (agonist)	11.0	−19.97	−16.75	3.22
				bezafibrate (agonist)	11.9	−23.69	−28.34	−4.65
				ciprofibrate (agonist)	12.1	−13.18	−11.87	1.31
				fenofibrate (agonist)	9.5	−26.60	−19.16	7.44
antithrombin-III (AT-III)	rs2227606	T147A	1NQ9[d]	heparin (potentiator)	7.0[e]		–[f]	
				sulodexide (potentiator)				
				tinzaparin (potentiator)				
butyrylcholinesterase (BCHE)	rs1799807	D70G	1P0M (1.69)	echothiophate (inhibitor)	5.8	−13.24	−3.54	9.70
				hexafluoronium (inhibitor)	4.8	−30.80	−23.66	7.14
beta-2 adrenergic receptor (ADRB2)	rs1800888	T164I	3D4S (0.53)	arformoterol (agonist)	7.7	−38.07	−34.43	3.64
				clenbuterol (agonist)	8.1	−28.96	−30.99	−2.03
				fenoterol (agonist)	8.5	−26.99	−26.47	0.52
				orciprenaline (agonist)	8.5	−11.15	−19.97	−8.82
				pirbuterol (agonist)	9.1	−18.78	−22.48	−3.70
				procaterol (agonist)	9.1	−25.25	−21.86	3.39
				salbutamol (agonist)	7.6	−26.65	−22.39	4.26
				terbutaline (agonist)	8.5	−17.78	−19.26	−1.48
plasminogen	rs4252186	H133Q	1CEA (1.02)	aminocaproic-acid (inhibitor)	8.0	−10.16	−8.86	1.30
				tranexamic-acid (inhibitor)	8.0	−13.21	−11.93	1.28
poly[ADP-ribose] polymerase-1 (PARP-1)	rs1136410	V762A	1WOK (1.16)	nicotinamide (binder)	12.0	−9.90	−7.13	2.77
glutamate receptor, ionotropickainate 1 (GRIK1)	rs363494	I727 V	2ZNS (0.85)	topiramate (antagonist)	7.8	−13.61	−31.71	−18.10
alcohol dehydrogenase (ADH)	rs2229540	N52S	2ALR[c]	fomepizole (inhibitor)	9.7	3.71	4.64	0.93
ferrochelatase (FECH)	rs3848519	R96Q	1HRK (4.03)	methyl-aminolevulinate (potentiator)	12.0		–[g]	
acetyl-CoA carboxylase 2 (ACC2)	rs2300455	A651T	3GID (0.42)	metformin (potentiator)	11.0	1.37	1.63	0.26
73-kDa molecular chaperone (HSP73)	rs11551602	D32Y	3FZM (4.08)	gentamicin (inhibitor)	10.1		–[g]	

[a]RMSD between the redocked pose and crystal pose of the co-crystallized ligand; it was defined as successful reproduction if the RMSD ≤ 2 Å. [b]Binding free energies calculated by the MM/GBSA approach, where $\Delta\Delta G = \Delta G_{MT} - \Delta G_{WT}$. WT and MT represent wild-type and mutant drug-target complexes, respectively. [c]Drug target with no co-crystallized ligand. [d]Drug target with very complex co-crystallized ligand that failed in the reproduce docking simulation. [e]Distance measured with the distance between co-crystallized ligand and SNP site. [f]Binding free energies cannot be calculated due to the complex structures or ambiguous binding sites of the drugs. [g]Binding free energies have not been calculated due to the unreliable redocking pose of the co-crystallized ligand.

Molecular Docking. X-ray crystal structures of drug targets were used as initial structures for molecular docking. The binding sites of the drug targets were determined with one of the two following criteria: (i) The position of the co-crystallized ligand was used as the active site when the co-crystallized ligand is available. (ii) The position of the co-crystallized ligand in a homology protein was mapped into the corresponding investigated target when there is no co-crystallized ligand in the target proteins, such as cytochrome P450 3A4 (CYP3A4) and alcohol dehydrogenase (ADH) in Table 1. After minimization, the drugs were docked into the targets by using the Autodock 4.2 program[14] with Lamarckian genetic algorithm (LGA).[15] The Gasteiger charge was applied to the macromolecules and drugs.[16] Each drug was docked 100 times, and the conformation with the highest docking score was chosen for both the drug-SNP site distance measurement and molecular dynamics (MD) simulation (for systems with drug-SNP site distance ≤12 Å). Mutations were introduced into the wild-type drug-target complexes by using the *biopolymer* module in SYBYL X1.2. A total of 42 complexes (21 wild-type and 21 mutated drug-target complexes) were collected as the initial structures for MD simulations.

Molecular Dynamics Simulation. The structure optimizations and electrostatic potential calculations of small-molecule drugs were both generated at the Hartree−Fock level with the 6-31G* basis set by using the Gaussian 03 program.[17] The partial atomic charges of these drugs were calculated using the RESP fitting method.[18] Amber99SB force field[19] and General Amber Force Field (GAFF)[20] were applied to the proteins and drugs, respectively. For the transmembrane protein (beta-2 adrenergic receptor), 1-palmytoil-2-oleoyl-sn-glycero-3-phosphatidylcholine (POPC) with the parameters

dx.doi.org/10.1021/ci400457v | J. Chem. Inf. Model. 2013, 53, 3343−3351

derived from Gould et al.[21] was used to construct the membrane systems. Counterions (Na^+ or Cl^-) were added to neutralize the systems. The nontransmembrane systems were then immersed in a TIP3P water box[22] within an 8 Å radius, whereas the transmembrane systems were first embedded in a well-equilibrated POPC membrane (a total of 217 lipid molecules) with the transmembrane region of the proteins parallel to the Z axis, followed by the addition of 15 Å thick TIP3P water to the $\pm Z$ axis out of the solute.

The MD simulations were carried out with NAMD version 2.8.[23] The particle mesh Ewald (PME) was used to calculate the long-range electrostatic interactions.[24] The cutoff distance of the short-range interaction was set to 10 Å. All hydrogen covalent bonds were constrained with the SHAKE algorithm.[25] The time step was set to 2 fs. A five-step minimization protocol was used prior to MD simulations. All atoms, except hydrogen, were initially constrained (2500 steps). Afterward, water molecules and ions (including lipid molecules) were able to move freely (2500 steps). The protein side chains were then also relaxed (2500 steps). Furthermore, the ligand and main-chain atoms within 5 Å of the mutated residue were permitted to move freely (2500 steps). Finally, movement was allowed for all the atoms (20,000 steps). In the MD simulation phase, the systems were gradually heated with the main protein chains constrained by 5 kcal/mol $Å^2$ in the NVT ensemble from 0 to 310 K. Next, 5 ns production runs were performed at 1 atm and at 310 K controlled by the Poisson Piston algorithm by using the NPT ensemble.[26] The atom coordinates were collected at intervals of 5 ps (200 frames/ns).

Binding Free Energy Calculation. The MM/GBSA methodology was applied to calculate the binding free energy.[27−35] Accordingly, the binding free energy of the drug-target complex was calculated using the following equations

$$\Delta G = G_{cpx} - (G_{rec} + G_{lig}) \quad (1)$$

$$G_{bind} = E_{MM} - TS + G_{solv} \quad (2)$$

$$E_{MM} = E_{int} + E_{elec} + E_{vdW} \quad (3)$$

$$G_{solv} = G_{GB} + G_{SA} \quad (4)$$

$$G_{SA} = \gamma A + b \quad (5)$$

where the G_{bind} term contains the molecular mechanism part (E_{MM}), entropy part ($-TS$), and solvation part (G_{solv}). The E_{MM} term includes the internal energy (E_{int}) (bond, angle, and dihedral energies) and intermolecular energy (electrostatic and van der Waals energies). G_{solv} is composed of electrostatic (G_{GB}) and nonpolar contributions (G_{SA}) to solvation, where G_{GB} and G_{SA} are calculated using the modified GB model[36] and eq 5, respectively. The A in eq 5 is the solvent-accessible surface area that was calculated using the LCPO algorithm,[37] and the parameters γ and b were set to 0.0072 and 0, respectively. The interior dielectric constant was set to 1.0, and the outer dielectric constant was set to 80.0. THe normal-mode analysis[38] was performed to estimate the conformational entropy changes of the drug-target complexes. A truncation of 12 Å within the ligands of the complexes were used for normal-mode analyses because of the expensive computational demand.[39] Drug-target interactions were partitioned per residue with the above-mentioned MM/GBSA parameters. The contribution of per drug-residue pair was calculated using the equilibrium trajectories of the complexes (the last 4 ns). All the MM/GBSA free energy calculations were performed using the *MMPBSA.py* module[40] in Ambertools 1.5.

RESULTS AND DISCUSSION

Structural Features of SNPs in Drug Targets. The 271 successful human drug targets were collected from TTD.[10] On the basis of the records in Ensembl BioMart,[41] these targets contain 473 synonymous and 406 nonsynonymous mutation sites. The minor allele frequency (MAF) data of 11 populations were obtained from the International HapMap Project.[13] The ratios of the nonsynonymous to synonymous (NS:S) sites for each MAF bin of 11 populations were calculated. The results show that the average NS:S ratios decrease with increasing MAF (Figure 1). This finding is highly similar to the recent

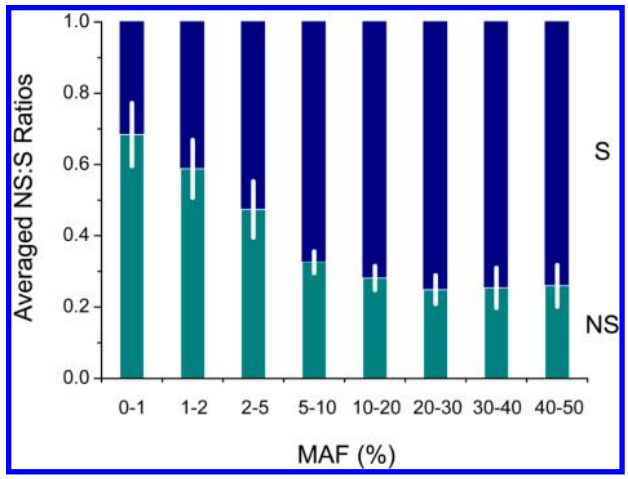

Figure 1. Averaged NS:S ratios (±SD) for different minor allele frequency (MAF) bins of drug targets. It is shown that with an increase in MAF, the NS:S ratio decreases, which suggests that drug targets are under strong purifying selection.

observation made by Nelson et al.[42] and suggests that drug targets undergo strong purifying selection because of their vital physiological functions.

A total of 69 out of 271 successful targets have structures recorded in the Protein Data Bank.[43] These structures contain active pockets and are thus appropriate for structural analyses to determine drug-target binding. These targets had a total of 158 SNPs with frequency information and were modulated by 238 approved drugs. Most of the drugs (232 out of 238) were successfully docked into their corresponding target. Here, we neglected the accuracy of the binding poses of the docked drugs because our purpose is to measure the distance between the docked drugs and the SNPs, which is insensitive to the binding poses of the docked drugs. A docking was marked success if drugs can be docked into the predefined binding site. Six drugs failed in the docking procedure due to various reasons, such as too many rotatable bonds of the drugs, covalently linked drugs, and ambiguous binding positions of the drugs where the queried drugs are too different from the co-crystallized ligands to determine their binding positions. The shortest distance between the heavy atoms of the drugs and mutated residues was measured. For the six drugs that failed in the docking, the shortest distance between co-crystallized ligands and mutated residues was measured instead. All of the results are listed in Table S1 of the Supporting Information. It is shown that most of the SNPs (92.4%) are located far from the drugs (>12 Å). However, 12 SNPs are located in close proximity to the drugs

dx.doi.org/10.1021/ci400457v | J. Chem. Inf. Model. 2013, 53, 3343−3351

Table 2. Validation of Docking/MD Strategy in ADRB2 and EGFR Systems

target/drug	PDB code	reproduced docking RMSD (Å)	ΔG_{bind} (kcal/mol)	K_d (nM)	IC_{50} (nM)
ADRB2/carazolol[a]	2RH1	0.99	–		
$EGFR_{wt}$/gefitinib	2ITO	1.99	−27.13	35.3[c]/53.5[d]	33[e]
$EGFR_{T790M\&L858R}$/gefitinib	4I22	1.17	−28.85	10.9[c]	–
$EGFR_{E746\_A750\_del}$/gefitinib[b]	–	–	−27.44	–	19[f]/39[g]/50[h]

[a]ADRB2 was only used for docking evaluation. [b]$EGFR_{E746\_A750\_del}$ was mutated from $EGFR_{wt}$. [c]K_d value from Yun et al. (2). [d]K_d value from Yun et al. (47). [e]IC_{50} value from Wakeling et al. (69). [f]IC_{50} value from Cheng et al. (71). [g]IC_{50} value from Li et al. (68). [h]IC_{50} value from Koizumi et al. (70).

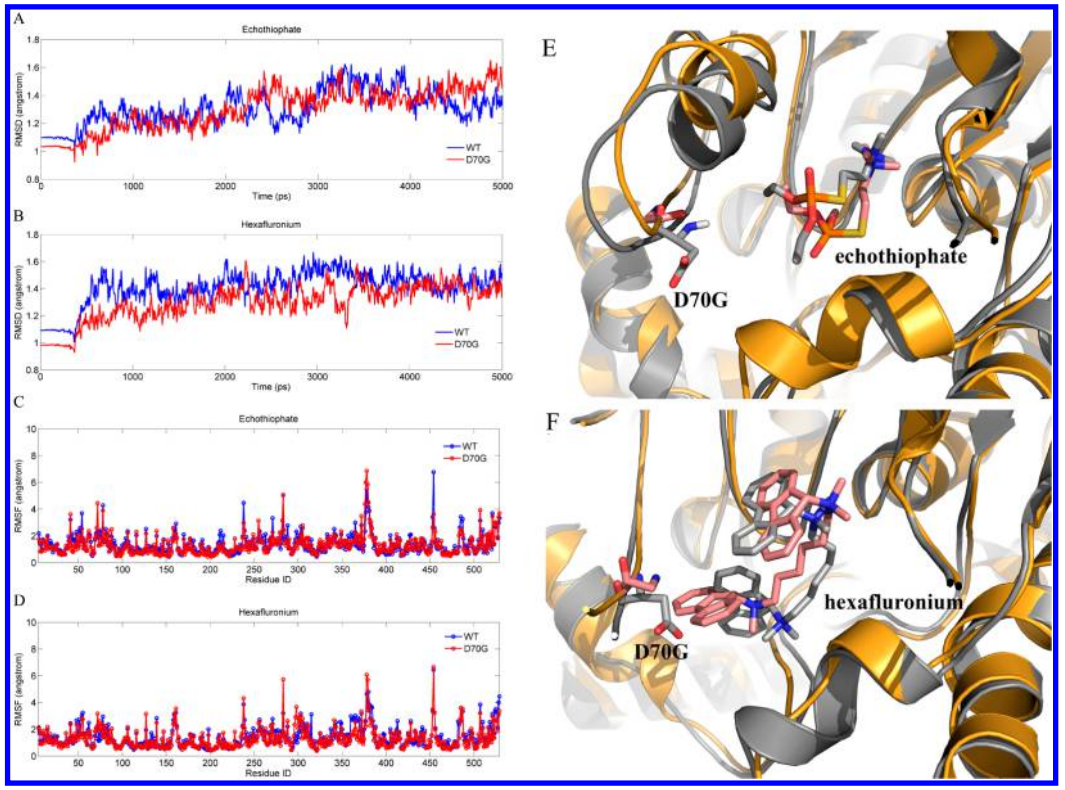

Figure 2. Stability of the BCHE systems over MD simulations. RMSDs (A for echothiophate and B for hexafluoronium) and most regions of RMSFs (C for echothiophate and D for hexafluoronium) are less than 1.6 and 2.0 Å, respectively, over the MD simulations (WT and MT BCHEs are colored in blue and red, respectively), and the averaged structures (E for echothiophate and F for hexafluoronium) are overlapped well between WT (gray in cartoon and stick models) and MT (orange in cartoon and pink in stick models) BCHEs, indicating that no significant conformational change has occurred in the mutated BCHE.

(≤12 Å, 7.6%), and one has a drug-SNP distance of less than 5 Å. These results are consistent with a recent finding that the occurrence rate of nonsynonymous SNPs at the active sites of proteins is lower than 1%.[44] Therefore, the unfavorable mutations near the protein pockets are largely purified, and most SNPs in the targets have negligible effects on drug binding. Nevertheless, a small number of nonsynonymous SNPs exist near the binding sites of drugs and may affect the interactions between drugs and targets. Therefore, a more detailed analysis on the binding free energy must be conducted.

Evaluation of Docking/MD Simulation Strategy. Prior to the analysis of the SNP effect on the binding of the drugs to the 12 drug targets that have SNPs near the binding site (drug-SNP distance ≤12 Å), we evaluated the reliability of the docking strategy to reproduce the binding poses of the co-crystallized ligands in the investigated drug targets and free energy calculation strategy to reproduce the ranking result of the experimental data in a well-known example of the SNP effect on gefitinib in a double mutant (T790 M and L858R) of epidermal growth factor receptor (EGFR). The reproduced docking poses of the co-crystallized ligands are available in the Supporting Information, and the RMSDs between the crystal pose and the docked pose of the co-crystallized ligand are summarized in Table 1. Nine out of 12 crystal structures were used to evaluate the reliability of docking results, and it was defined as a successful reproduction if the RMSD was less than 2 Å.[30,45] It can be found that the binding poses of the co-crystallized ligands in 7 out of 9 crystal structures (78%) could be successfully reproduced with the RMSD between crystal pose and docked pose ≤2 Å, which is consistent with Li's result that approximate 80% of the crystal binding poses could be reproduced by Autodock 4.2,[46] and two crystal structures (FECH and HSP73) that failed in the reproduction (RMSD > 4 Å) were abandoned in the further MD simulation and free energy analysis. Additionally, two well-known systems were used to validate our calculation procedure. One is the b2-adrenergic receptor (ADRB2) co-crystallized with carazolol (PDB code 2RH1), and the other is wild-type EGFR (PDB code 2ITO) and its double mutant (T790 M and L858R, PDB code 4I22) co-crystallized with gefitinib, which have also been

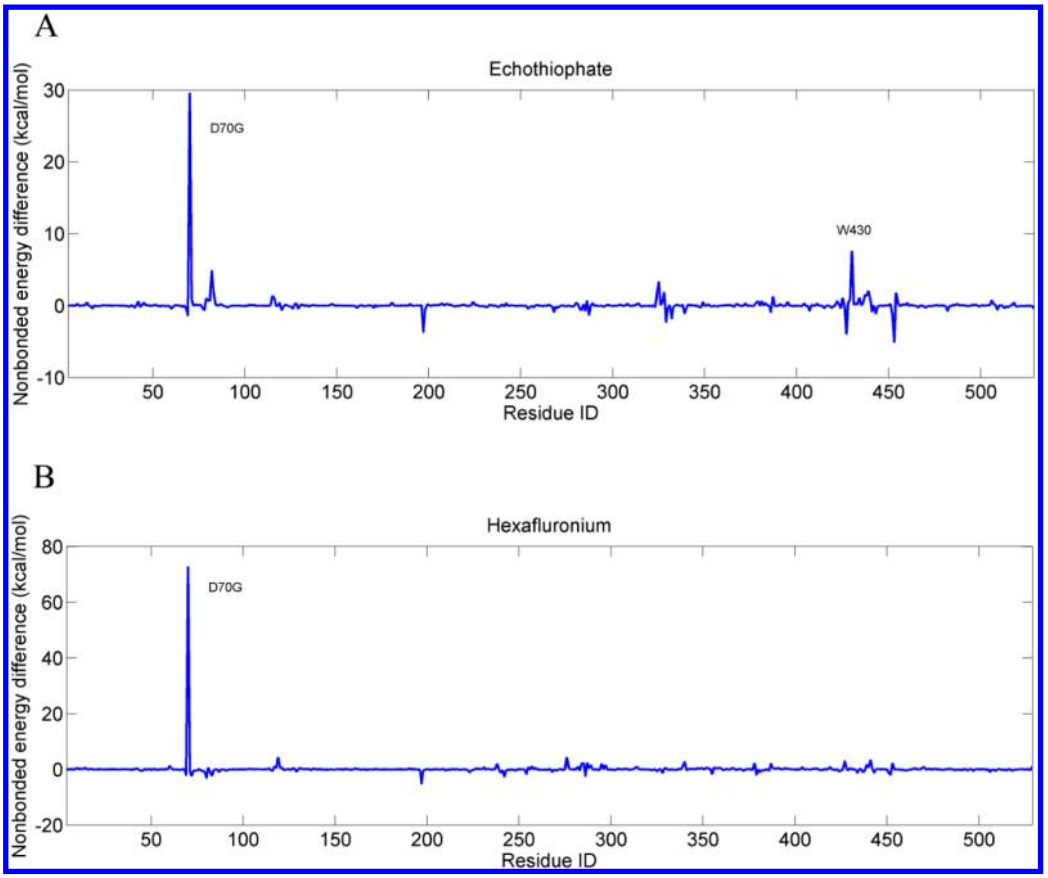

Figure 3. Differences in contribution of residues to the nonbonded binding energy between the wild-type (WT) and D70G mutant (MT) of BCHE. $\Delta E = E_{MT} - E_{WT}$. A positive value of ΔE indicates a weaker binding affinity in the mutant protein, while a negative value of ΔE indicates a stronger binding affinity. (A) binding with echothiophate; (B) binding with hexafluoronium.

used in the free energy strategy evaluation. The reproduced RMSDs were all less than 2 Å as shown in Table 2. As mentioned above, MD simulation and MM/GBSA free energy calculation were applied to the EGFR systems (wild-type and its T790M&L858R mutant). The top scored docking poses, which have a RMSD of 1.99 and 1.17 Å for wild-type and mutant$_{T790M\&L858R}$ EGFRs, respectively, were used to validate the docking/free energy calculation strategy (the structures can be found in Web site: http://ibi.hzau.edu.cn/download/PDB.rar). As shown in Table 2, the calculated binding free energy of the wild-type and mutant$_{T790M\&L858R}$ EGFRs are consistent with the experiment data[2,47] and previous studies that used a similar procedure to ours.[48] Therefore, the present strategy is appropriate for the evaluation of SNP effects on drug-target binding (the detailed information can be found in Table S2, Supporting Information).

Energetic Features of SNPs in Drug Targets. A total of 26 chemical drugs have been approved for the 12 SNP-containing targets located near the binding pockets (≤12 Å). Twenty-one out of the 26 drugs were successfully docked into the corresponding targets. Three drugs, namely, heparin, tinzaparin, and sulodexide, failed to dock because of their complex structures (for heparin and tinzaparin) and ambiguous binding sites (for sulodexide), and the other two drugs, methyl-aminolevulinate and gentamicin, were abandoned due to the failure of reproducing the crystal binding pose (Table 1). The top-scoring conformations of the drug-target complexes were used as initial structures for MD simulation and MM/GBSA free energy calculations.[30,46]

The MM/GBSA calculation results are summarized in Table 1. The contribution of each energy term to the total binding free energy is listed in Table S2 of the Supporting Information. Note that the binding free energies of 10 drugs (~50%) are weakly affected by the mutations, and an energy difference of less than 3 kcal/mol is observed between wild-type and mutant targets. This value indicates that nearly half of the drugs are not significantly affected by the near-pocket SNPs. However, five drugs, which all have an energy difference of more than 7 kcal/mol, may be strongly affected by the mutations. In particular, echothiophate, hexafluoronium, and fenofibrate exhibit decreased binding free energies for the mutated targets, whereas the other two, namely, orciprenaline and topiramate, have enhanced affinities to the mutant targets. The relationships between agonist/antagonist binding affinities and their therapeutic effects are highly complicated.[49−53] Therefore, the effects of the mutant target on fenofibrate, orciprenaline (which are agonists), and topiramate (an antagonist) are difficult to predict. However, for enzyme-targeting inhibitors, a lowered drug binding affinity generally implies weakened therapeutic effects. Thus, the D70G mutation in butyrylcholinesterase (BCHE) is expected to attenuate the effects of echothiophate and hexafluoronium. This inference is supported by the BCHE D70G mutation-induced resistance to echothiophate and mivacurium, a cognate of hexafluoronium.[54,55] As shown in Figure 2, the BCHE systems are stable over the whole MD simulations with the RMSDs (Figure 2A and B). Most regions of RMSFs (Figure 2C and D) are less than 1.6 and 2 Å, respectively, and no significant conformational change was

dx.doi.org/10.1021/ci400457v | J. Chem. Inf. Model. 2013, 53, 3343−3351

observed in the mutated BCHE (Figure 2E and F), indicating that the mutation D70G can hardly affect the conformational change of the protein. Further analysis of MM/GBSA calculation results indicate that the effects of D70G mutation on the binding affinities of echothiophate and hexafluoronium are dominated by nonbonded energies ($\Delta G_{nonbonded}$) (Table S2, Supporting Information). These energies are significantly decreased by the absence of the negatively charged residue D70 that could increase the Coulomb interaction to the positively charged drugs echothiophate (+1 charge) and hexafluoronium (+2 charges), as clearly shown in the residue contributions to the nonbonded binding energies (Figure 3).

Implications for Drug Therapy. Because the frequency of the D70G mutation in BCHE is highest in the Toscans of Italy (TSI, up to 4%) (Table S1, Supporting Information), echothiophate and hexafluoronium should be used with caution in this population. By comparison, the D70G mutation in BCHE is very rare (near zero) in the Han Chinese of Beijing (CHB), Japanese of Tokyo (JPT), and Yoruba of Ibadan (YRI) (Table S1, Supporting Information), which suggests that the administration of these drugs is relatively safe in these populations. Therefore, the present results can direct population-based drug therapy, when combined with SNP frequency information from different populations.

More importantly, the present results have implications for chemical treatment of genetic diseases. Up to now, approximate 19,000 kinds of genetic diseases have been determined,[56,57] and many of them are recommended to be treated with gene therapy for the reason that these diseases are heritable.[58,59] However, it is still a great challenge to treat genetic diseases with "gene repair".[58,59] Alternatively, small molecular drugs are also feasible in genetic disease treatment.[60] The rationale is that the diseases arising from gain of function (GOF) mutation of certain genes may be ameliorated by antagonists targeting these genes. On the contrary, diseases coming from loss of function (LOF) mutations may be treated by agonists of the target genes.[61] However, a premise for this chemical strategy to treat genetic diseases is that the GOF/LOF mutations in drug targets have negligible influence on drug-target binding, which is supported by the present analyses on structural and energetic features of SNPs in drug targets. This chemical strategy is validated by the treatment of squamous-cell carcinoma of the head and neck (SCCHN), a rare tumor entity occurring in about 0.7/1,000,000 inhabitants in the United States.[62] This disease arises from the GOF mutation in the epidermal growth factor receptor (EGFR),[63] a famous target in the treatment of various cancers.[64] Two launched drugs targeting EGFR, i.e., gefitinib (a small-molecule drug) and cetuximab (a monoclonal antibody), show promising benefit in the treatment of SCCHN by inhibiting the activated EGFR mutant[64−67] without losing binding affinity compared with the wild-type EGFR.[68−71] Therefore, it is promising to perform chemical treatments to genetic diseases through combining the information of pathogenesis of genetic diseases (GOF/LOF) and the action mechanisms (as antagonists or agonists) of the existent drugs. The above instance has also been validated by our docking/MD strategy. As shown in Table 2, the binding free energy of gefitinib to the wild-type EGFR is very similar to that of mutated $EGFR_{E746\_A750\_del}$ (−27.13 kcal/mol in wild-type and −27.44 kcal/mol in $mutant_{E746\_A750\_del}$, respectively, detailed information can be found in Table S2, Supporting Information), indicating that the mutated target is still sensitive to gefitinib, which is consistent with the experimental result.[68−71]

By comparing the 406 nonsynonymous mutations with the mutations recorded in OMIM,[57] we found that 24 mutations in 21 targets are linked to genetic diseases (Table S3, Supporting Information). The indications of drugs for these targets were manually compared with the genetic disease traits, which revealed three matches between them (Table 3). Thus, these drugs are of great potential to combat the corresponding genetic diseases. For instance, the R788C mutation of voltage-dependent T-type calcium channel subunit alpha-1H (CACNA1H) induces epilepsy by GOF. Because flunarizine, which targets CACNA1H as an inhibitor, has a therapeutic effect on epilepsy, it is reasonable to infer that flunarizine may be used to treat the inheritable epilepsy through suppressing the function of CACNA1H that was enhanced by R788C mutation. Likewise, ardeparin, which targets heparin cofactor 2 as an agonist, is promising to treat inheritable deep vein thrombosis induced by R189H mutation of the target because this LOF mutation is associated with heparin cofactor II deficiency, which leads to increased thrombin generation. The crystal structure of heparin cofactor 2 (PDB code 1JMO) indicates that the R189H mutation is located ∼20 Å away from the covalently linked ardeparin-like ligand (Table S1, Supporting Information), which means that the mutation will not affect the binding of the drug. Pioglitazone, rosiglitazone, and troglitazone that target peroxisome proliferator activated receptor gamma (PPARG) as agonists may be effective to treat genetic diabetes mellitus induced by the P12A mutation of the target because this LOF mutation is associated with diabetes mellitus.

Table 3. Drug-Target Genes with SNPs and Indications Matched with Genetic Disease Genes

	CACNA1H	SERPIND1	PPARG
SNP ID	rs3751664	rs5907	rs1801282
protein allele	R788C	R189H	P12A
OMIM ID	607904.0004	142360.0001	601487.0002
OMIM traits	childhood absence epilepsy	heparin cofactor II deficiency	type II diabetes mellitus
pathogenesis	GOF	LOF	LOF
approved drugs	flunarizine	ardeparin	pioglitazone rosiglitazone troglitazone
drug mode of action	inhibitor	agonist	agonist
drug indication	epilepsy	deep vein thrombosis	type II diabetes mellitus

CONCLUSIONS

In conclusion, the structural and energy properties of SNPs in successful drug targets were analyzed. The structural features of the SNPs indicated that most SNPs (92.4%) are located far from the drug-binding site (>12 Å). Furthermore, energy calculations revealed that only a minority of SNPs near the binding pocket can seriously affect drug binding. Thus, combined with SNP frequency information from different populations, these results will be beneficial to population-based drug therapy. Besides, the slight influence of SNPs on drug-target binding has significant implications for chemical therapy of genetic diseases. To this end, one should take into consideration the pathogenesis (GOF or LOF mutations) of the diseases and the drug mode of action (antagonists or agonists) as well.

■ ASSOCIATED CONTENT

Supporting Information

Table S1: Basic information on the 69 targets and 158 SNPs. Table S2: Detailed information of the binding free energies of drug-target complexes using the MM/GBSA approach (kcal/mol, standard deviation is in parentheses). Table S3: The 24 disease-causing genetic mutations in 21 drug-target genes. All of the docked crystal structures and final coordinate pdb files of MD runs are available at Web site http://ibi.hzau.edu.cn/download/PDB.rar. This material is available free of charge via the Internet at http://pubs.acs.org.

■ AUTHOR INFORMATION

Corresponding Author

*E-mail: zhy630@mail.hzau.edu.cn. Fax: +86 27 87280877.

Present Addresses

[‖]H.-Y.S.: Institute of Functional Nano & Soft Materials (FUNSOM) and Jiangsu Key Laboratory for Carbon-Based Functional Materials & Devices, Soochow University, Suzhou, Jiangsu 215123, China.

[⊥]F.-Q.J.: Key Laboratory of Pesticide and Chemical Biology Ministry of Education, College of Chemistry, Central China Normal University, Wuhan 430079, China.

Author Contributions

[§]H.-Y.S. and F.-Q.J.: These authors contributed equally to this work.

Notes

The authors declare no competing financial interest.

■ ACKNOWLEDGMENTS

This work was supported by the National Basic Research Program of China (973 Project, Grants 2010CB126100 and 2012CB721000), National Natural Science Foundation of China (Grants 21173092 and 31201952), and Natural Science Foundation of Hubei Province (Grant 2013CFA016).

■ REFERENCES

(1) Gorre, M. E.; Mohammed, M.; Ellwood, K.; Hsu, N.; Paquette, R.; Rao, P. N.; Sawyers, C. L. Clinical resistance to STI-571 cancer therapy caused by BCR-ABL gene mutation or amplification. *Science* **2001**, *293*, 876−880.

(2) Yun, C.-H.; Mengwasser, K. E.; Toms, A. V.; Woo, M. S.; Greulich, H.; Wong, K.-K.; Meyerson, M.; Eck, M. J. The T790M mutation in EGFR kinase causes drug resistance by increasing the affinity for ATP. *Proc. Natl. Acad. Sci. U.S.A.* **2008**, *105*, 2070−2075.

(3) Choi, Y. L.; Soda, M.; Yamashita, Y.; Ueno, T.; Takashima, J.; Nakajima, T.; Yatabe, Y.; Takeuchi, K.; Hamada, T.; Haruta, H. EML4-ALK mutations in lung cancer that confer resistance to ALK inhibitors. *N. Engl. J. Med.* **2010**, *363*, 1734−1739.

(4) Sun, H. Y.; Ji, F. Q. A molecular dynamics investigation on the crizotinib resistance mechanism of C1156Y mutation in ALK. *Biochem. Biophys. Res. Commun.* **2012**, *423*, 319−324.

(5) Sun, H.; Li, Y.; Li, D.; Hou, T. Insight into crizotinib resistance mechanisms caused by three mutations in ALK tyrosine kinase using free energy calculation approaches. *J. Chem. Inf. Model.* **2013**, *53*, 2376−2389.

(6) Karczewski, K. J.; Daneshjou, R.; Altman, R. B. Chapter 7: Pharmacogenomics. *PLoS Comput. Biol.* **2012**, *8*, e1002817.

(7) Kell, D. B.; Dobson, P. D.; Bilsland, E.; Oliver, S. G. The promiscuous binding of pharmaceutical drugs and their transporter-mediated uptake into cells: What we (need to) know and how we can do so. *Drug Discovery Today* **2013**, *18*, 218−239.

(8) Sachidanandam, R.; Weissman, D.; Schmidt, S. C.; Kakol, J. M.; Stein, L. D.; Marth, G.; Sherry, S.; Mullikin, J. C.; Mortimore, B. J.; Willey, D. L. A map of human genome sequence variation containing 1.42 million single nucleotide polymorphisms. *Nature* **2001**, *409*, 928−933.

(9) Wood, A. J. J.; Evans, W. E.; McLeod, H. L. Pharmacogenomics—Drug disposition, drug targets, and side effects. *N. Engl. J. Med.* **2003**, *348*, 538−549.

(10) Zhu, F.; Shi, Z.; Qin, C.; Tao, L.; Liu, X.; Xu, F.; Zhang, L.; Song, Y.; Zhang, J. Therapeutic target database update 2012: A resource for facilitating target-oriented drug discovery. *Nucleic Acids. Res.* **2012**, *40*, 1128−1136.

(11) Sayers, E. W.; Barrett, T.; Benson, D. A.; Bolton, E.; Bryant, S. H.; Canese, K.; Chetvernin, V.; Church, D. M.; DiCuccio, M.; Federhen, S. Database resources of the national center for biotechnology information. *Nucleic Acids. Res.* **2011**, *39*, 38−51.

(12) Apweiler, R.; Martin, M.; O'Donovan, C.; Magrane, M.; Alam-Faruque, Y.; Antunes, R.; Barrell, D.; Bely, B.; Bingley, M.; Binns, D. The universal protein resource (UniProt) in 2010. *Nucleic Acids. Res.* **2010**, *38*, 142−148.

(13) Gibbs, R. A.; Belmont, J. W.; Hardenbol, P.; Willis, T. D.; Yu, F.; Yang, H.; Ch'ang, L. Y.; Huang, W.; Liu, B.; Shen, Y. The international HapMap project. *Nature* **2003**, *426*, 789−796.

(14) Morris, G. M.; Huey, R.; Lindstrom, W.; Sanner, M. F.; Belew, R. K.; Goodsell, D. S.; Olson, A. J. AutoDock4 and AutoDockTools4: Automated docking with selective receptor flexibility. *J. Comput. Chem.* **2009**, *30*, 2785−2791.

(15) Morris, G. M.; Goodsell, D. S.; Halliday, R. S.; Huey, R.; Hart, W. E.; Belew, R. K.; Olson, A. J. Automated docking using a Lamarckian genetic algorithm and an empirical binding free energy function. *J. Comput. Chem.* **1998**, *19*, 1639−1662.

(16) Gasteiger, J.; Marsili, M. Iterative partial equalization of orbital electronegativity—a rapid access to atomic charges. *Tetrahedron* **1980**, *36*, 3219−3228.

(17) Frisch, M.; Trucks, G.; Schlegel, H.; Scuseria, G.; Robb, M.; Cheeseman, J.; Montgomery Jr, J.; Vreven, T.; Kudin, K.; Burant, J. Gaussian 03; Gaussian, Inc.: Wallingford, CT, 2004.

(18) Bayly, C. I.; Cieplak, P.; Cornell, W.; Kollman, P. A. A well-behaved electrostatic potential based method using charge restraints for deriving atomic charges: The RESP model. *J. Phys. Chem.* **1993**, *97*, 10269−10280.

(19) Wang, J.; Cieplak, P.; Kollman, P. A. How well does a restrained electrostatic potential (RESP) model perform in calculating conformational energies of organic and biological molecules? *J. Comput. Chem.* **2000**, *21*, 1049−1074.

(20) Wang, J.; Wolf, R. M.; Caldwell, J. W.; Kollman, P. A.; Case, D. A. Development and testing of a general amber force field. *J. Comput. Chem.* **2004**, *25*, 1157−1174.

(21) Dickson, C. J.; Rosso, L.; Betz, R. M.; Walker, R. C.; Gould, I. R. GAFFlipid: A General Amber Force Field for the accurate molecular dynamics simulation of phospholipid. *Soft Matter* **2012**, *8*, 9617−9627.

(22) Jorgensen, W. L.; Chandrasekhar, J.; Madura, J. D.; Impey, R. W.; Klein, M. L. Comparison of simple potential functions for simulating liquid water. *J. Chem. Phys.* **1983**, *79*, 926−935.

(23) Phillips, J. C.; Braun, R.; Wang, W.; Gumbart, J.; Tajkhorshid, E.; Villa, E.; Chipot, C.; Skeel, R. D.; Kale, L.; Schulten, K. Scalable molecular dynamics with NAMD. *J. Comput. Chem.* **2005**, *26*, 1781−1802.

(24) Darden, T.; York, D.; Pedersen, L. Particle mesh Ewald: An N log(N) method for Ewald sums in large systems. *J. Chem. Phys.* **1993**, *98*, 10089−10092.

(25) Ryckaert, J. P.; Ciccotti, G.; Berendsen, H. J. C. Numerical integration of the cartesian equations of motion of a system with constraints: molecular dynamics of n-alkanes. *J. Comput. Phys.* **1977**, *23*, 327−341.

(26) Feller, S. E.; Zhang, Y.; Pastor, R. W.; Brooks, B. R. Constant-pressure molecular-dynamics simulation-the Langevin piston method. *J. Chem. Phys.* **1995**, *103*, 4613−4621.

(27) Hou, T.; Li, N.; Li, Y.; Wang, W. Characterization of domain−peptide interaction interface: Prediction of SH3 domain-mediated

protein−protein interaction network in yeast by generic structure-based models. *J. Proteome Res.* **2012**, *11*, 2982−2995.
(28) Hou, T.; Li, Y.; Wang, W. Prediction of peptides binding to the PKA RIIα subunit using a hierarchical strategy. *Bioinformatics* **2011**, *27*, 1814−1821.
(29) Hou, T.; Wang, J.; Li, Y.; Wang, W. Assessing the performance of the MM/PBSA and MM/GBSA methods: I. The accuracy of binding free energy calculations based on molecular dynamics simulations. *J. Chem. Inf. Model.* **2011**, *51*, 69−82.
(30) Hou, T.; Wang, J.; Li, Y.; Wang, W. Assessing the performance of the molecular mechanics/Poisson Boltzmann surface area and molecular mechanics/generalized Born surface area methods. II. The accuracy of ranking poses generated from docking. *J. Comput. Chem.* **2011**, *32*, 866−877.
(31) Hou, T.; Yu, R. Molecular dynamics and free energy studies on the wild-type and double mutant HIV-1 protease complexed with amprenavir and two amprenavir-related inhibitors: mechanism for binding and drug resistance. *J. Med. Chem.* **2007**, *50*, 1177−1188.
(32) Li, L.; Li, Y.; Zhang, L.; Hou, T. Theoretical studies on the susceptibility of oseltamivir against variants of 2009 A/H1N1 influenza neuraminidase. *J. Chem. Inf. Model.* **2012**, *52*, 2715−2729.
(33) Xu, L.; Sun, H.; Li, Y.; Wang, J.; Hou, T. Assessing the performance of MM/PBSA and MM/GBSA methods. 3. The impact of force fields and ligand charge models. *J. Phys. Chem. B* **2013**, *117*, 8408−8421.
(34) Xue, W.; Jin, X.; Ning, L.; Wang, M.; Liu, H.; Yao, X. Exploring the molecular mechanism of cross-resistance to HIV-1 integrase strand transfer inhibitors by molecular dynamics simulation and residue interaction network analysis. *J. Chem. Inf. Model.* **2013**, *53*, 210−222.
(35) Zhang, J.; Hou, T.; Wang, W.; Liu, J. S. Detecting and understanding combinatorial mutation patterns responsible for HIV drug resistance. *Proc. Natl. Acad. Sci. U.S.A.* **2010**, *107*, 1321−1326.
(36) Onufriev, A.; Bashford, D.; Case, D. A. Exploring protein native states and large-scale conformational changes with a modified generalized born model. *Proteins: Struct., Funct., Bioinf.* **2004**, *55*, 383−394.
(37) Weiser, J.; Shenkin, P. S.; Still, W. C. Approximate atomic surfaces from linear combinations of pairwise overlaps (LCPO). *J. Comput. Chem.* **1999**, *20*, 217−230.
(38) Brooks, B.; Karplus, M. Harmonic dynamics of proteins: Normal modes and fluctuations in bovine pancreatic trypsin inhibitor. *Proc. Natl. Acad. Sci. U.S.A.* **1983**, *80*, 6571−6575.
(39) Genheden, S.; Kuhn, O.; Mikulskis, P.; Hoffmann, D.; Ryde, U. The normal-mode entropy in the MM/GBSA method: Effect of system truncation, buffer region, and dielectric constant. *J. Chem. Inf. Model.* **2012**, *52*, 2079−2088.
(40) Miller, B. R., III; McGee, T. D.; Swails, J. M.; Homeyer, N.; Gohlke, H.; Roitberg, A. E. MMPBSA.py: An efficient program for end-state free energy calculations. *J. Chem. Theory Comput.* **2012**, *8*, 3314−3321.
(41) Flicek, P.; Amode, M. R.; Barrell, D.; Beal, K.; Brent, S.; Chen, Y.; Clapham, P.; Coates, G.; Fairley, S.; Fitzgerald, S. Ensembl 2011. *Nucleic Acids. Res.* **2011**, *39*, 800−806.
(42) Nelson, M. R.; Wegmann, D.; Ehm, M. G.; Kessner, D.; Jean, P. S.; Verzilli, C.; Shen, J.; Tang, Z.; Bacanu, S. A.; Fraser, D. An abundance of rare functional variants in 202 drug target genes sequenced in 14,002 people. *Science* **2012**, *337*, 100−104.
(43) Bernstein, F. C.; Koetzle, T. F.; Williams, G. J. B.; Meyer, E. F.; Brice, M. D.; Rodgers, J. R.; Kennard, O.; Shimanouchi, T.; Tasumi, M. The protein data bank. *Eur. J. Biochem.* **2008**, *80*, 319−324.
(44) Dingerdissen, H.; Motwani, M.; Karagiannis, K.; Simonyan, V.; Mazumder, R. Proteome-wide analysis of nonsynonymous single-nucleotide variations in active sites of human proteins. *FEBS J.* **2013**, *280*, 1542−1562.
(45) Wang, R.; Lu, Y.; Wang, S. Comparative evaluation of 11 scoring functions for molecular docking. *J. Med. Chem.* **2003**, *46*, 2287−2303.
(46) Hou, x.; Du, J.; Zhang, J.; Du, L.; Fang, H.; Li, M. How to improve docking accuracy of AutoDock4.2: A case study using different electrostatic potentials. *J. Chem. Inf. Model.* **2013**, *53*, 188−200.
(47) Yun, C.-H.; Boggon, T. J.; Li, Y.; Woo, M. S.; Greulich, H.; Meyerson, M.; Eck, M. J. Structures of lung cancer-derived EGFR mutants and inhibitor complexes: mechanism of activation and insights into differential inhibitor sensitivity. *Cancer cell* **2007**, *11*, 217−227.
(48) Balius, T. E.; Rizzo, R. C. Quantitative prediction of fold resistance for inhibitors of EGFR. *Biochemistry* **2009**, *48*, 8435−8448.
(49) Mahfoudi, A.; Roulet, E.; Dauvois, S.; Parker, M. G.; Wahli, W. Specific mutations in the estrogen receptor change the properties of antiestrogens to full agonists. *Proc. Natl. Acad. Sci. U.S.A.* **1995**, *92*, 4206−4210.
(50) Rajendra, S.; Lynch, J. W.; Pierce, K. D.; French, C. R.; Barry, P. H.; Schofield, P. R. Mutation of an arginine residue in the human glycine receptor transforms β-alanine and taurine from agonists into competitive antagonists. *Neuron* **1995**, *14*, 169−175.
(51) Turki, J.; Lorenz, J. N.; Green, S. A.; Donnelly, E. T.; Jacinto, M.; Liggett, S. B. Myocardial signaling defects and impaired cardiac function of a human beta 2-adrenergic receptor polymorphism expressed in transgenic mice. *Proc. Natl. Acad. Sci. U.S.A.* **1996**, *93*, 10483−10488.
(52) Bessis, A.-S.; Rondard, P.; Gaven, F.; Brabet, I.; Triballeau, N.; Prézeau, L.; Acher, F.; Pin, J.-P. Closure of the Venus flytrap module of mGlu8 receptor and the activation process: Insights from mutations converting antagonists into agonists. *Proc. Natl. Acad. Sci. U.S.A.* **2002**, *99*, 11097−11102.
(53) Dishy, V.; Landau, R.; Sofowora, G. G.; Xie, H.-G.; Smiley, R. M.; Kim, R. B.; Byrne, D. W.; Wood, A. J.; Stein, C. M. Beta2-adrenoceptor Thr164Ile polymorphism is associated with markedly decreased vasodilator and increased vasoconstrictor sensitivity in vivo. *Pharmacogenetics* **2004**, *14*, 517−522.
(54) Boeck, A. T.; Fry, D. L.; Sastre, A.; Lockridge, O. Naturally occurring mutation, Asp70His, in human butyrylcholinesterase. *Ann. Clin. Biochem.* **2002**, *39*, 154−156.
(55) Masson, P.; Froment, M.; Bartels, C.; Lockridge, O. Importance of aspartate-70 in organophosphate inhibition, oxime re-activation and aging of human butyrylcholinesterase. *Biochem. J.* **1997**, *325*, 53−61.
(56) Amberger, J.; Bocchini, C. A.; Scott, A. F.; Hamosh, A. McKusick's online Mendelian inheritance in man (OMIM®). *Nucleic Acids. Res.* **2009**, *37*, 793−796.
(57) Hamosh, A.; Scott, A. F.; Amberger, J. S.; Bocchini, C. A.; McKusick, V. A. Online Mendelian Inheritance in Man (OMIM), a knowledgebase of human genes and genetic disorders. *Nucleic Acids. Res.* **2005**, *33*, 514−517.
(58) O'Connor, T. P.; Crystal, R. G. Genetic medicines: Treatment strategies for hereditary disorders. *Nat. Rev. Genet.* **2006**, *7*, 261−276.
(59) Fischer, A.; Cavazzana-Calvo, M. Gene therapy of inherited diseases. *Lancet* **2008**, *371*, 2044−2047.
(60) Melnikova, I. Rare diseases and orphan drugs. *Nat. Rev. Drug Discovery* **2012**, *11*, 267−268.
(61) Brinkman, R. R.; Dubé, M.-P.; Rouleau, G. A.; Orr, A. C.; Samuels, M. E. Human monogenic disorders—A source of novel drug targets. *Nat. Rev. Genet.* **2006**, *7*, 249−260.
(62) Krengli, M.; Jereczek-Fossa, B. A.; Kaanders, J. H.; Masini, L.; Beldi, D.; Orecchia, R. What is the role of radiotherapy in the treatment of mucosal melanoma of the head and neck? *Crit. Rev. Oncol. Hematol.* **2008**, *65*, 121−128.
(63) Lee, J. W.; Soung, Y. H.; Kim, S. Y.; Nam, H. K.; Park, W. S.; Nam, S. W.; Kim, M. S.; Sun, D. I.; Lee, Y. S.; Jang, J. J. Somatic mutations of EGFR gene in squamous cell carcinoma of the head and neck. *Clin. Cancer Res.* **2005**, *11*, 2879−2882.
(64) Mendelsohn, J.; Baselga, J. Status of epidermal growth factor receptor antagonists in the biology and treatment of cancer. *J. Clin. Oncol.* **2003**, *21*, 2787−2799.
(65) Perez, C. A.; Song, H.; Raez, L. E.; Agulnik, M.; Grushko, T. A.; Dekker, A.; Stenson, K.; Blair, E. A.; Olopade, O. I.; Seiwert, T. Y. Phase II study of gefitinib adaptive dose escalation to skin toxicity in recurrent or metastatic squamous cell carcinoma of the head and neck. *Oral Oncol.* **2012**, *48*, 887−892.

(66) Cohen, E. E.; Rosen, F.; Stadler, W. M.; Recant, W.; Stenson, K.; Huo, D.; Vokes, E. E. Phase II trial of ZD1839 in recurrent or metastatic squamous cell carcinoma of the head and neck. *J. Clin. Oncol.* **2003**, *21*, 1980−1987.
(67) Bonner, J. A.; Harari, P. M.; Giralt, J.; Azarnia, N.; Shin, D. M.; Cohen, R. B.; Jones, C. U.; Sur, R.; Raben, D.; Jassem, J. Radiotherapy plus cetuximab for squamous-cell carcinoma of the head and neck. *N. Engl. J. Med.* **2006**, *354*, 567−578.
(68) Li, Z.; Zhou, S.; Zhang, L.; Su, C.; Hang, J.; Zhao, Y.; Su, B.; Zhou, C. BIM induction of apoptosis triggered by EGFR-sensitive and resistance cell lines of non-small-cell lung cancer. *Med. Oncol.* **2011**, *28*, 572−577.
(69) Wakeling, A. E.; Guy, S. P.; Woodburn, J. R.; Ashton, S. E.; Curry, B. J.; Barker, A. J.; Gibson, K. H. ZD1839 (Iressa) an orally active inhibitor of epidermal growth factor signaling with potential for cancer therapy. *Cancer Res.* **2002**, *62*, 5749−5754.
(70) Koizumi, F.; Shimoyama, T.; Taguchi, F.; Saijo, N.; Nishio, K. Establishment of a human non-small cell lung cancer cell line resistant to gefitinib. *Int. J. Cancer* **2005**, *116*, 36−44.
(71) Cheng, H.; An, S. J.; Dong, S.; Zhang, Y. F.; Zhang, X. C.; Chen, Z. H.; Su, J.; Wu, Y. L. Molecular mechanism of the schedule-dependent synergistic interaction in EGFR-mutant non-small cell lung cancer cell lines treated with paclitaxel and gefitinib. *J. Hematol. Oncol.* **2011**, *4*, 5−17.